

19. S. B. Altner, M. Mitsunaga, G. Zumofen, U. P. Wild, *Phys. Rev. Lett.* **76**, 1747 (1996).
20. R. Brown, M. Orrit, in *Single Molecule Optical Detection, Imaging and Spectroscopy* (VCH, Weinheim, Germany, 1997), pp. 109–142.
21. T. Richter, *Opt. Acta* **29**, 265 (1982).
22. A. Beige, G. C. Hegerfeldt, *Phys. Rev. A* **58**, 4133 (1998).
23. T. Basché, W. E. Moerner, M. Orrit, H. Talon, *Phys. Rev. Lett.* **69**, 1516 (1992).
24. In our experiment, the detection of a photon is accompanied by populating the molecular ground state via fast decay of vibrational levels. As a result, all of the information about the phase of the system is lost, and we can assume that after the first photon has been detected, the only nonzero elements of the density matrix are the populations $\rho_{eg,eg}$, $\rho_{ge,ge}$, and $\rho_{gg,gg}$.
25. G. Whitesides, B. Grzybowski, *Science* **295**, 2418 (2002).
26. M. E. Davis, *Nature* **417**, 813 (2002).
27. S. Lloyd, *Science* **261**, 1569 (1993).
28. X. Hu, K. Schulten, *Phys. Today* **50**, 28 (1997).
29. We thank C. Henkel and G. Zumofen for fruitful

discussions and J. Mlynek for continuous support. We are also grateful to M. Orrit for bringing our attention to the discussion on excitation-induced frequency shifts. The experimental part of this project was performed before we moved from the University of Konstanz, and we thank the Deutsche Forschungsgemeinschaft (SFB 513) as well as the European Union (grant S4P) for financial support.

1 July 2002; accepted 26 August 2002
Published online 5 September 2002;
10.1126/science.1075606
Include this information when citing this paper.

REPORTS

High Abrasion Resistance with Sparse Mineralization: Copper Biomineral in Worm Jaws

Helga C. Lichtenegger,^{1*} Thomas Schöberl,² Michael H. Bartl,¹ Herbert Waite,^{3*} Galen D. Stucky^{1*}

Biominerals are widely exploited to harden or stiffen tissues in living organisms, with calcium-, silicon-, and iron-based minerals being most common. In notable contrast, the jaws of the marine bloodworm *Glycera dibranchiata* contain the copper-based biomineral atacamite [$\text{Cu}_2(\text{OH})_3\text{Cl}$]. Polycrystalline fibers are oriented with the outer contour of the jaw. Using nanoindentation, we show that the mineral has a structural role and enhances hardness and stiffness. Despite the low degree of mineralization, bloodworm jaws exhibit an extraordinary resistance to abrasion, significantly exceeding that of vertebrate dentin and approaching that of tooth enamel.

Most living organisms rely on hard tissues for support, protection, nutrition, and defense. Biomineralization is a major strategy for tissue hardening and manifests an astonishing diversity of bioceramic structures with exquisite microarchitectures that have specially adapted physical properties (1–6). Although the variety of architectures seems to be almost infinite, Ca-, Si-, and Fe-based minerals are most common (7). As a basic principle, the hardness of these is largely governed by the type of mineral (8) and the degree of mineralization (9, 10).

In 1980, Gibbs and Bryan (11) first reported copper levels up to 13% w/w in the jaws of the marine polychaete worm *Glycera* sp. Although it was initially suspected that these levels reflected heavy metal pollution at the collection site, jaw composition was found to be remarkably consistent and independent of copper concentration in the seawater. Copper was the most abundant inor-

ganic component; protein, however, was the most predominant constituent (measured as percent of dry weight). The authors concluded that the copper might play a role in mechanically hardening the proteinaceous material. However, no attempt to determine the actual hardness was made nor was the form of the copper further explored.

We show that in *Glycera* jaws, a major part of the copper is deposited as a biomin-

eral. We used a combination of techniques, such as position-resolved synchrotron x-ray diffraction, small-angle scattering, electron microscopy, and nanoindentation to identify the mineral, demonstrate its structural function, and probe the mechanical properties of the jaw. We find that, in spite of the low degree of mineralization, *Glycera* jaws show an extraordinary resistance to abrasion.

Figure 1A shows the image of a *Glycera* jaw as viewed by light microscopy. *Glycera* is armed with a set of four such jaws, each of which is about 1.5 mm long and jet black, with a very sharp, mechanically stable tip that is used by the worm to penetrate the integument of its prey (12) and inject venom (13). Electron microprobe experiments (14) on a ground and polished *Glycera* jaw showed high concentrations of copper in the distalmost tip region (Fig. 1). In accordance with findings by Gibbs and Bryan (1980) (11), the copper concentration decreased dramatically from the tip to the base. The local copper distribution in an oblique cross section of the tip is depicted in Fig. 1B (the dark hole in the middle is the venom canal, and the white line circumscribes the outline of the sample). Figure 1C shows the local chlorine distribution. The occurrence of chlorine in the sample was highly correlated with elevated local concentrations of copper (additional chlo-

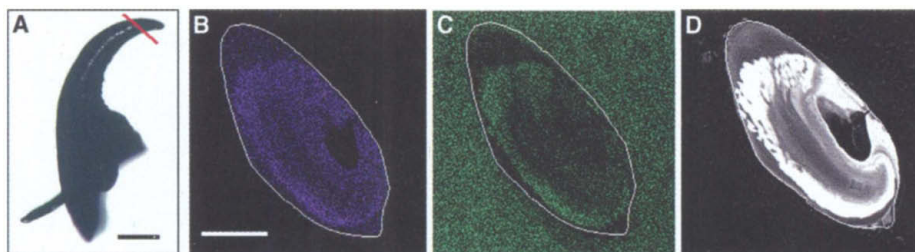


Fig. 1. (A) Picture of a *Glycera* jaw under the light microscope. The sharp tip of the jaw is used to penetrate prey integument and inject venom. *Glycera* worms were obtained live from the Marine Biological Laboratory in Woods Hole, Massachusetts, and jaws were dissected from the animal after freezing. The scale bar corresponds to 0.2 mm. The red line denotes the plane of cross section used for element analysis. (B) Electron microprobe, copper dot map. The white line denotes the outline of the sample. Scale bar, 50 μm . Regions with higher copper concentration appear bright. The dark region in the middle corresponds to the venom canal. (C) Electron microprobe, chlorine dot map. The distribution of chlorine in the sample is highly correlated with the distribution of copper as seen from the copper dot map (additional chlorine around the sample belongs to the epoxy embedding). (D) Backscattered electron image. Regions containing high concentrations of elements with larger Z appear bright. The image shows that the inner part of the jaw tip is highly mineralized, in accordance with the element dot map of copper.

¹Department of Chemistry and Biochemistry, University of California, Santa Barbara, CA 93106, USA. ²Erich Schmid Institute for Materials Science, Austrian Academy of Sciences and University of Leoben, Jahnstrasse 12, A-8700 Leoben, Austria. ³Department of Molecular, Cellular and Developmental Biology, University of California, Santa Barbara, CA 93106, USA.

*To whom correspondence should be addressed.

rine around the sample in this picture is derived from the epoxy embedding). Except for the tip, the rest of the sample did not contain detectable levels of chlorine. Backscattered electron imaging (BEI) was used as a complementary technique to visualize the copper distribution. The contrast is due to differences in atomic number Z , with bright regions indicating heavier elements. The BEI image (Fig. 1D) is in perfect agreement with the copper distribution obtained from the electron microprobe element map.

The structure of the copper agglomerations in the *Glycera* jaw tip was studied by x-ray diffraction (XRD) on dried jaws at the Advanced Photon Source (APS) of the Argonne National Laboratory (ANL). Experimental details are given as supporting online material (14). The experiment revealed a crystalline phase in the tip region of the jaw

(Fig. 2A). The same pattern was also found in fresh frozen specimens when examined with conventional XRD. Bragg reflections were observed only in a region of about 200 to 300 μm around the end of the tip. An excellent match in position and intensity of the peaks in the diffraction pattern was obtained with the calculated pattern of the copper- and chlorine-containing mineral atacamite (15) [$\text{Cu}_2(\text{OH})_3\text{Cl}$] (dashed line in Fig. 2B). The compound $\text{Cu}_2(\text{OH})_3\text{Cl}$ occurs in four polymorphs: atacamite, botallackite, paratacamite, and clinatacamite. None of the other three polymorphs matched the diffraction data. The mineral atacamite is known to form under two extreme environmental conditions: in very arid climates [the main location is the Atacama Desert, Chile (16)] and in seawater (17). Both environments ensure the stability

of atacamite, which is otherwise soluble in fresh water (17). The hardness of atacamite is slightly greater than that of calcite (18).

Transmission electron microscopy (TEM) on thin sections of the jaw tip revealed that the atacamite is organized in fibers (dark regions denoting higher electron density, Fig. 3A) within a protein matrix (light gray, Fig. 3A). For details on sample preparation and measurement, see materials and methods (14). Mineralized fibers are arranged in layers, with the very surface and some inner parts being free of mineral. A similar distribution can be seen in the backscattered electron image in Fig. 1D, where bright regions indicating greater mineralization do not extend to the very surface, and the mineral is not evenly distributed in the jaw tip. In Fig. 3B, long mineralized fibers are shown in greater magnification. Energy-dispersive x-ray analysis in single fibers and between fibers showed that most of the copper is concentrated in the fibers. In Bragg contrast (dark-field TEM, Fig. 3C), the same sample showed bright spots at various places in the fibers, where the illumination changed quickly to other spots along the fiber upon tilting, as different lattice planes of the mineral fulfilled the diffraction condition. This suggests that the fibers are polycrystalline, consisting of single crystallites in a size range from 10 to 50 nm, as estimated from the size of the single bright spots in Fig. 3C. The large size of the single crystals is also in agreement with the observation of very sharp reflections in XRD (compare Fig. 2A), whereas the polycrystallinity explains the presence of rings in the XRD pattern (Fig. 2A), indicating a rather random crystallographic orientation. The insert in Fig. 3C, top right corner, shows a selected area electron diffraction pattern from part of a fiber. The diffraction pattern corresponds to that of atacamite and displays reflections from more than one single crystallite. In contrast, TEM micrographs from the base of the jaws had no fiberlike structure, but the sample was homogenous with a low electron density.

Small-angle x-ray scattering (SAXS) studies at the APS, ANL (14) showed that the mean fiber orientation throughout the tip is roughly parallel to its outer shape. This can be concluded from the fact that the short axis of the SAXS pattern (Fig. 4A, top) always followed the outer contour of the jaw tip (compare sketch in Fig. 4, left; the red circle indicates the size of the x-ray beam). Quantitative evaluation of the SAXS patterns yielded a mean fiber diameter of 81 ± 14 nm (19), which is in excellent agreement with the fiber diameter obtained from scanning electron microscopy (SEM) (Fig. 4B top) on a fracture surface in the tip region and TEM (Fig. 3). In the rest of the jaw, the fracture surface as viewed by SEM exhibited a less pronounced, rather random structure (Fig. 4B, bottom), and the SAXS signal was isotropic and vanishingly weak (Fig. 4A, bottom). For experimental details, refer to the materials and methods (14).

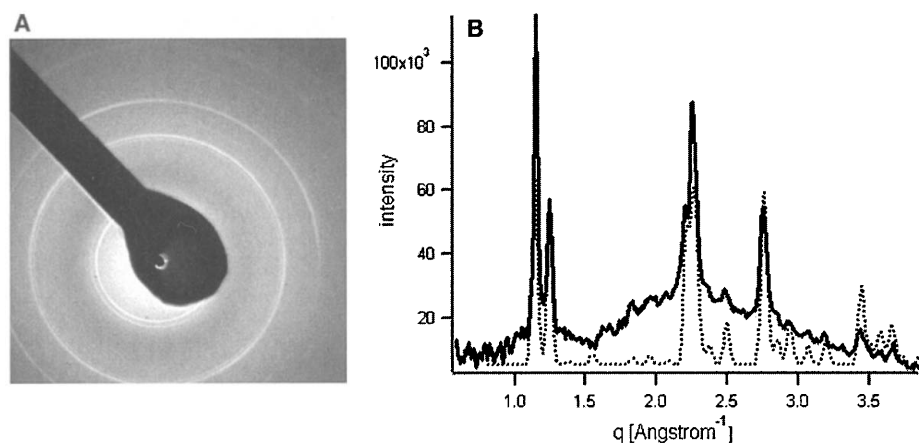


Fig. 2. (A) Synchrotron x-ray diffraction on *Glycera* jaws revealed strong Bragg reflections in the tip of the jaw. (B) Integration of the diffraction data over the azimuth angle yielded a diffraction curve (solid line). The comparison with the calculated pattern of the copper- and chlorine-containing mineral atacamite (dotted line) [$\text{Cu}_2(\text{OH})_3\text{Cl}$] gave excellent agreement. The data are plotted versus the scattering vector q , with $q = \frac{4\pi}{\lambda} \sin\theta$, where λ is the wavelength of the incident beam and 2θ is the scattering angle.

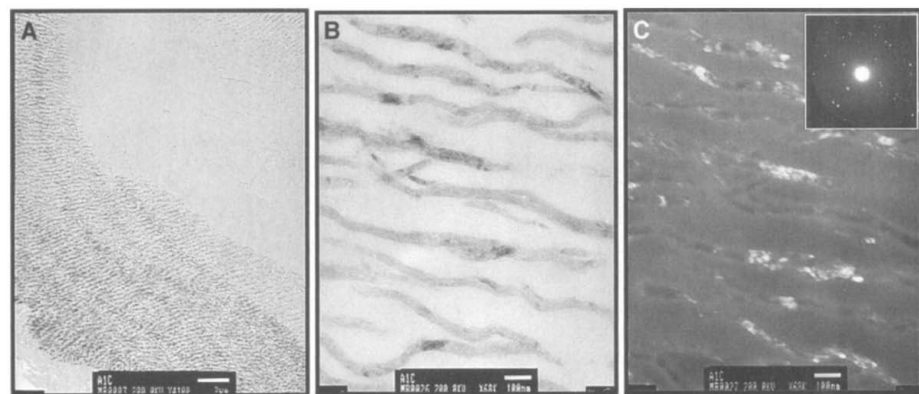


Fig. 3. TEM images of thin sections of a *Glycera* jaw tip. (A) Mineralized fibers (dark) are embedded in a protein matrix (light gray). Fibers are found in certain layers only. The surface layer (lower left corner) and parts further inside the tip (upper right corner) are free of mineral. Scale bar, 2 μm . (B) Long fibers under higher magnification. Scale bar, 100 nm. (C) Dark-field TEM image (Bragg contrast) of the same sample shown in (B). Crystallites that fulfill the diffraction conditions appear as bright spots. Scale bar, 100 nm. The inset in the top right corner shows a selected area electron diffraction pattern from part of a fiber.

REPORTS

In order to investigate whether the copper-based mineral in *Glycera* jaws has a hardening effect on the material, nanoindentation experiments and microprobe element analysis were carried out on the same sample, as described in the materials and methods (14). A longitudinal section of a *Glycera* jaw was indented in an array of 5- μm steps at the very tip and 10- μm steps in the rest of the sample. Hardness H and elastic modulus (stiffness) E were determined at each point (20) and arranged into two-dimensional maps in pseudo-gray scale (Fig. 5, A and B): Bright regions denote high values and dark regions low values of H and E , respectively. The pixel size of the maps corresponds to 5 μm , with missing values obtained by interpolation. Electron microprobe analysis on the same sample after indentation showed that the regions with higher H and E , such as the tip and regions near the surface, were indeed those containing more copper. Figure 5, C and D, show a copper dot map and a backscattered electron image, respectively. Microprobe analysis was also used to determine the copper and chlorine concentration quantitatively at selected points. The intensities of the characteristic copper and chlorine radiations were compared to those obtained from standard samples with known weight % of copper and chlorine and corrected for absorption and atomic number effects. Details are given as supporting online material (14). The mineral volume % was calculated from the copper and chlorine concentrations, taking into account the atomic ratio of Cu:Cl = 2:1 in atacamite and approximate mineral and matrix densities (14). Because there was more copper than expected in this ratio, the chlorine content was taken as an indicator of mineral content. Figure 5, E and F, show that H as well as E increased with increasing mineral content (solid circles denote experimental data).

Considering the structure of the *Glycera* jaw as a fiber composite consisting of hard fibers in a softer protein matrix, it is possible to obtain rough quantitative estimates for H and E as a function of mineral content (fiber volume fraction), using simple model calculations as outlined in the supporting online material (14). The increase of a material's hardness by addition of hard particles is extremely dependent on the particle shape (21). The least pronounced hardening effect is obtained with spherical particles (dashed line in Fig. 5E), the strongest with long cylinders when loaded parallel to the axis (Fig. 5E, dashed line, cylinder aspect ratio 10) (21). Cylinders with an aspect ratio of 0.1 (discs) would lead to an intermediate hardening effect (Fig. 5E, solid line). The experimental data also lie in an intermediate range. E values were calculated according to the Halpin-Tsai approximation (22, 23) for fiber composites. The dotted line in Fig. 5F represents an upper limit given by long fibers loaded parallel to their axis and the dashed line a lower limit corresponding to long fibers loaded in a transverse direction.

The experimental data lie well in between these two limits. The solid line in Fig. 5F shows an approximation to the data, assuming a fiber aspect ratio of 10 and parallel loading.

In Table 1, the mechanical properties of *Glycera* jaws are compared with those of enamel and dentin in vertebrate teeth (24, 25). In spite of its low degree of mineralization, the

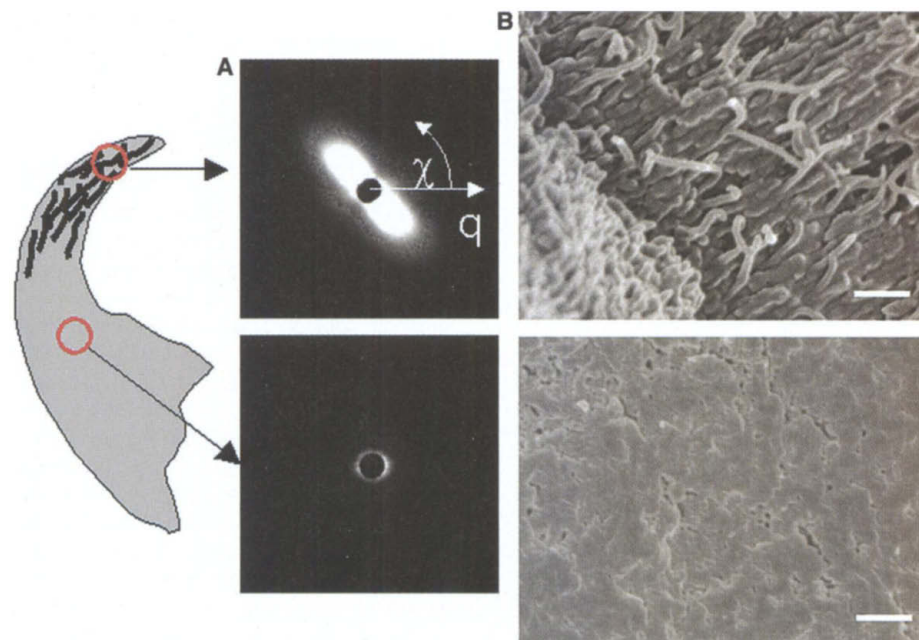
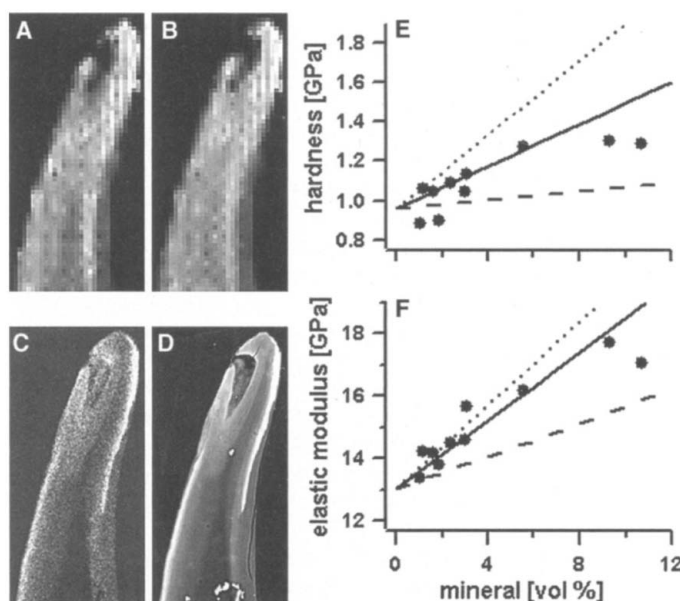


Fig. 4. (Left) Model of the arrangement of mineralized fibers in *Glycera* jaws. The fibers are elongated and oriented along the outer contour of the tip. The red circles denote the size of the synchrotron x-ray beam (100 μm). (A) SAXS on wet *Glycera* jaws. The top image shows the scattering pattern obtained from the tip. Note the strong anisotropic signal. The signal from the rest of the sample (bottom image) almost vanished except at very small angles. (B) SEM images of fracture surfaces. Top: fibrous structure in tip of jaw. Bottom: irregular structure in rest of jaw. Scale bars, 1 μm .

Fig. 5. (A) Hardness map of *Glycera* jaw tip obtained by nanoindentation. Pixel size, 5 μm . Bright regions indicate greater hardness. (B) Map of E . (C) Electron microprobe analysis. The copper dot map shows local copper concentration. Bright regions contain more copper. (D) Backscattered electron image. Bright regions contain a larger amount of elements with higher Z, here copper. (E) Hardness versus mineral content, calculated from the copper and chlorine concentration measured quantitatively with microprobe analysis at selected points. The hardness increases with increasing mineral content.



Comparison of the experimental data (solid circles) with model calculations (solid, dashed, and dotted lines) shows that the experimental hardness values lie in between the calculated lower bound (reinforcement with spherical particles, dashed line) and upper bound (long fibers loaded parallel to the fiber axis, dotted line). The solid line models a system containing disks loaded parallel to the cylinder axis. (F) E versus mineral content. Higher E values are related to a larger amount of mineral. The dotted and dashed lines represent theoretical E values for two extreme cases, respectively: long fiberlike particles loaded parallel to the longitudinal axes (upper limit) and in a transverse direction (lower limit). The data can be approximated, assuming fibers with an aspect ratio of 10 in parallel loading condition (solid line).

REPORTS

Table 1. Mechanical properties and degree of mineralization in *Glycera* jaws as compared to human dentin and enamel. For the *Glycera* jaw, the minimum, maximum, and mean values of *H* and *E* (350 indents) are shown.

Material	<i>H</i> (GPa)	<i>E</i> (GPa)	<i>H</i> ^{3/2} / <i>E</i>	Volume % mineral
<i>Glycera</i> jaw				
Minimum	0.89	13.42	0.063	1.03
Mean	1.11	15.16	0.077	3.95
Maximum	1.31	17.75	0.084	9.29
Dentin (24, 25)	0.65–1	19.5–27.7	0.027–0.036	70
Enamel (24)	4.74	100.8	0.103	96

Table 2. Amino acid composition of *Glycera* and *Nereis* jaw tips in residues per 1000 residues (standard error ± 5% for five analyses). Except for the histidine content, the observed composition of *Glycera* jaws resembles that found in an earlier analysis (12). The histidine difference is undoubtedly due to the use of the jaw tips alone in the present study.

Amino acid	<i>Glycera</i>	<i>Nereis</i>
Asp	5	119
Thr	3	8
Ser	5	24
Glu	7	73
Pro	4	16
Gly	632	377
Ala	7	39
Cys/2	0	0
Val	3	10
Met	0	>1
Ile	1	10
Leu	1	9
Tyr	1	80
Phe	1	17
His	325	191
Lys	2	14
Arg	2	10
Total	999	1000

Glycera jaw is considerably harder than dentin but not as hard as enamel. *E* of the *Glycera* jaw is below that of enamel and dentin. Although high hardness and stiffness are often regarded as desirable material characteristics per se, it is commonly understood that the resistance of a material to abrasion correlates rather with the ratio of *H*^{3/2}/*E* (26). Table 1 shows that the *H*^{3/2}/*E* ratio in *Glycera* jaws was more than double that of dentin and reached 80% of that of enamel, with a degree of mineralization that is 1/17 that of dentin and 1/24 that of enamel. This is particularly remarkable given enamel's excellent resistance to wear and abrasion (10, 24, 27).

Copper is well known for its pivotal role in enzyme catalysis (28), but its participation in the integrity of biostructural scaffolds is less familiar. Certain types of lichen may produce copper-containing mineral inclusions (moolooite) in the course of their erosion of copper-rich rocks (29). In the *Glycera* jaw, however, copper clearly plays a structural role. Although copper was present mainly as mineral deposits, the Cu:Cl ratio as determined by electron microprobe analysis was

considerably higher than in the mineral atacamite, pointing toward a substantial amount of excess copper. It has been found that cations of copper, iron, and zinc can, by coordination with multiple ligands, function as noncovalent cross-linkers of polymers (30) and protein scaffolds in normal and diseased tissues (31). Such a role was proposed to be the primary function of Zn in the jaws of the clamworm *Nereis* (32, 33), a close relative of *Glycera*. In *Nereis* jaws, however, there was no detectable crystalline form of Zn (34). The amino acid compositions of *Nereis* and *Glycera* jaws are similar in being dominated by two amino acids, glycine and histidine (Table 2); the latter is known to play an important role in metal binding (28). Details on the protein analysis are available as supporting online material (14).

It is noteworthy that in the *Glycera* jaw, the copper was not evenly distributed but occurred at higher concentrations in the inner part of the jaw rather than on the surface (compare Fig. 1D). A gradual increase of stiffness from the surface to the bulk has been shown to mitigate crack formation and to enhance the resistance of stiff materials to contact damage (35, 36). *Glycera* is a raptorial but rather indiscriminating carnivore that hunts by burrowing in marine sediments. Given that its jaws are as likely to close on a bit of gravel as they are on living tissue, mitigating contact damage appears crucial. The marriage of protein with copper mineral as well as with bound copper ions is an intriguing concept per se but may also serve as a design prototype for new materials that need to be hard, lightweight, and durable. The extraordinary selectivity for copper as compared to other transition metals in *Glycera* jaws, however, suggests an additional biological function beyond mechanical support. One possible explanation is that copper may mediate the activation of venom during injection. Indeed, other fibrous protein networks exhibit catalytic activity with bound copper (37, 38).

References and Notes

- J. Aizenberg, A. Tkachenko, S. Weiner, L. Addadi, G. Hendler, *Nature* **412**, 819 (2001).
- L. Addadi, S. Weiner, *Nature* **411**, 753 (2001).
- S. Kamat, X. Su, R. Ballarini, A. H. Heuer, *Nature* **405**, 1036 (2000).
- S. Mann, *Nature* **365**, 499 (1993).
- J. N. Cha et al., *Proc. Natl. Acad. Sci. U.S.A.* **96**, 361 (1999).
- W. J. Landis, *Connect. Tissue Res.* **35**, 1 (1996).

- H. A. Lowenstam, S. Weiner, *On Biomineralization* (Oxford Univ. Press, New York, 1989).
- H. A. Lowenstam, *Science* **156**, 1373 (1967).
- J. D. Currey, *J. Exp. Biol.* **202**, 3285 (1999).
- N. E. Waters, in *The Mechanical Properties of Biological Materials*, J. F. V. Vincent, J. D. Currey, Eds. (Cambridge Univ. Press, London, 1980), vol. 34, pp. 99–136.
- P. E. Gibbs, G. W. Bryan, *J. Mar. Biol. Assoc. UK* **60**, 205 (1980).
- C. Michel, M. T. Fonce-Vignaux, M. F. Voss-Foucart, *Bull. Biol. Fr. Belg.* **107**, 301 (1973).
- M. Thieffry, C. Bon, R. Manaranche, B. Saliou, M. Israel, *J. Physiol.* **78**, 343 (1982).
- Materials and methods are available as supporting material on Science Online.
- Powder Diffraction File: PDF 25-269*.
- M. C. Bandy, *Am. Mineral.* **23**, 669 (1938).
- M. D. Hannington, *Can. Mineral.* **31**, 945 (1993).
- W. L. Roberts, *Encyclopedia of Minerals* (Van Nostrand Reinhold, New York, ed. 2, 1990).
- P. Fratzl, *J. Stat. Phys.* **77**, 125 (1994).
- W. C. Oliver, G. M. Pharr, *J. Mater. Res.* **7**, 1564 (1992).
- G. Bao, J. W. Hutchinson, R. M. McMeeking, *Acta Metall. Mater.* **39**, 1871 (1991).
- J. E. Ashton, J. C. Halpin, P. H. Petit, *Primer in Composite Materials: Analysis* (Technomic Publishing, Stamford, CT, 1969), pp. 77–82.
- R. M. Jones, *Mechanics of Composite Materials* (Taylor and Francis, Philadelphia, ed. 2, 1999).
- H. Fong, M. Sarikaya, S. N. White, M. L. Snead, *Mater. Sci. Eng. C Biomimetic Supramolecular Syst.* **7**, 119 (2000).
- W. Tesch et al., *Calcified Tissue Int.* **69**, 147 (2001).
- B. Bhushan, *Principles and Applications of Tribology* (Wiley, New York, 1999).
- J. F. V. Vincent, *Structural Biomaterials* (Princeton Univ. Press, Princeton, NJ, 1990).
- R. H. Holm, P. Kennepohl, E. I. Solomon, *Chem. Rev.* **96**, 2239 (1996).
- J. E. Chisholm, G. C. Jones, O. W. Purvis, *Mineral. Mag.* **51**, 715 (1987).
- R. Krämer, J. M. Lehn, A. MarquisRigault, *Proc. Natl. Acad. Sci. U.S.A.* **90**, 5394 (1993).
- E. Vaccaro, J. H. Waite, *Biomacromolecules* **2**, 906 (2001).
- G. W. Bryan, P. E. Gibbs, *J. Mar. Biol. Assoc. UK* **59**, 969 (1979).
- _____, *J. Mar. Biol. Assoc. UK* **60**, 641 (1980).
- H. C. Lichtenegger, T. Schöberl, M. H. Bartl, H. Waite, G. D. Stucky, data not shown.
- S. Suresh, M. Olsson, A. E. Giannakopoulos, N. P. Padture, J. Jitcharoen, *Acta Mater.* **47**, 3915 (1999).
- S. Suresh, *Science* **292**, 2447 (2001).
- C. C. Curtin et al., *J. Biol. Chem.* **276**, 20466 (2001).
- N. Shiraishi, M. Nishikimi, *FEBS Lett.* **511**, 118 (2002).
- We thank the Complex Materials Consortium—Collaborative Access Team, D. M. Casa, Th. Gog, and C. Venkataraman, beamline 9-ID, APS, ANL, for their excellent support with the synchrotron experiments; D. Pierce, Department of Geological Sciences, University of California Santa Barbara (UCSB), for help with the microprobe experiment; J. Tang, Department of Chemistry, UCSB, for support with the SEM measurements; J. T. Ruokolainen, Department of Engineering, UCSB, for cutting samples for nanoindentation and TEM; and F. Zok, Department of Engineering, UCSB, for carefully reading our manuscript and valuable discussions. Use of the APS was supported by the U.S. Department of Energy, Office of Science, Office of Basic Energy Sciences, under contract no. W-31-109-Eng-38. We gratefully acknowledge support from the Office of Naval Research and the Biomaterials Program at NIH—National Institute of Dental and Craniofacial Research. H.C.L. was supported by the Fonds zur Förderung der Wissenschaftlichen Forschung (FWF), Austria. This work made use of MRL Central Facilities at UCSB supported by NSF under award no. DMR 00-80034. We gratefully acknowledge support from NSF under award no. DMR 96-34396.

Supporting Online Material
www.sciencemag.org/cgi/content/full/298/5592/389/DC1
 Materials and Methods
 References

25 June 2002; accepted 29 August 2002